9

Wood Technology/Products

Demiao Chu*, Xiaochuan Ren, Stavros Avramidis, Yong Zhu, Vahid Nasir, Sohrab Rahimi and Shengquan Liu

Mechanistic insights into enhanced fire and smoke resistance in surface densified wood: a chemical-free thermophysical approach

https://doi.org/10.1515/hf-2025-0069 Received May 28, 2025; accepted July 24, 2025; published online September 17, 2025

Abstract: Wood is a sustainable material, but its inherent flammability and smoke emissions limit its practical applications. This study proposes a thermo-physical strategy to enhance fire safety by fabricating surface densified wood (SDW). SDW were fabricated via hydrothermal pretreatment (20-80 °C) followed by thermo-densification, yielding samples with varying compression ratios (10-30 %; e.g., SDW₂₀-30 %) and deformation stabilities (e.g., SDW₈₀-30 %). Cone calorimetry revealed that the densified-surface-layer effectively suppressed heat and smoke release by promoting early char formation, which acted as a thermal and mass transfer barrier. SDW₂₀-30 % showed 20 % and 70 % reductions in total heat release (THR) and total smoke production (TSP) within the first 360 s. Further improvements were achieved with enhanced densified-surface-layer's stability: compared to SDW₂₀-30 %, SDW₈₀-30 % exhibited 32 %, 14 %, and 22 % reductions in CO yield, THR, and TSP, respectively, and delayed peak heat release rate by 73 s. Correlation analysis indicated that densified-surface-layer's deformation stability contributed more significantly to fire hazard mitigation than densification degree. Thermal and chemical analyses confirmed increased crystallinity and compositional evolution in the densified-surface-layer, leading to improved thermal resistance. These findings demonstrate a chemical-free approach to improving wood fire safety and offer insights into the development of safer bio-based materials.

Keywords: surface densification; thermo-modification; fire resistance; smoke suppression; poplar wood

1 Introduction

Wood is a naturally abundant and sustainable material with considerable potential in composite manufacturing, offering advantages in terms of environmental sustainability and structural properties (Huang et al. 2023). The growing use of timber in building construction presents a unique opportunity to promote greener, more sustainable construction practices (Ahn et al. 2022; Kumar et al. 2024). Engineered wood composites products and mass timber elements have revolutionized the construction industry, enabling the development of mid- and high-rise timber buildings (Goubran et al. 2020). These advancements offer sustainable alternatives to traditional materials like concrete and steel, providing both environmental benefits and enhanced structural efficiency. However, the inherent flammability of wood and wood-based composites to fire-related hazards remain significant challenges to their widespread application in advanced structural and engineering contexts (Ayanleye et al. 2022; Östman et al. 2017).

The increasing emphasis on sustainable materials highlights the potential of solid wood as a renewable, high-performance candidate for engineering applications (Ahn et al. 2022). To mitigate its natural flammability, wood is commonly treated with fire retardants through impregnation or surface coating, utilizing various chemical agents such as

Xiaochuan Ren, Yong Zhu and Shengquan Liu, Key Laboratory of National Forestry and Grassland Administration on Wood Quality Improvement & Efficient Utilization, School of Materials and Chemistry, Anhui Agricultural University, Hefei 230036, China, E-mail: rxcyjs@163.com (X. Ren), 2271834097@foxmail.com (Y. Zhu), liusq@ahau.edu.cn (S. Liu) Stavros Avramidis and Sohrab Rahimi, Department of Wood Science, University of British Columbia, Vancouver, BC, V6T 1Z4, Canada, E-mail: stavros.avramidis@ubc.ca (S. Avramidis), sohrab.rahimi@alumni.ubc.ca (S. Rahimi). https://orcid.org/0000-0001-6640-6626 (S. Rahimi)

Vahid Nasir, Department of Wood Science and Engineering, Oregon State University, Corvallis, OR 97331, USA, E-mail: vahid.nasir@oregonstate.edu

^{*}Corresponding author: Demiao Chu, Key Laboratory of National Forestry and Grassland Administration on Wood Quality Improvement & Efficient Utilization, School of Materials and Chemistry, Anhui Agricultural University, Hefei 230036, China, E-mail: Demiaochu@ahau.edu.cn. https://orcid.org/0009-0004-2525-1559

halogenated compounds, as well as boron- and nitrogenbased formulations (Sauerbier et al. 2020). However, many of these fire retardants, particularly halogenated phosphorus-based compounds, raise serious concerns regarding human health, environmental impact, and overall sustainability (Chen et al. 2020; Chen and Wang 2010; Dasari et al. 2013). Furthermore, the application of these fire retardants is often associated with practical limitations, such as reduced long-term effectiveness, poor compatibility with wood-based materials, and the need for energy-intensive processing. For instance, Harada et al. (2007) challenged the durability of ceramic coatings applied to fire-retardant wood, and Baysal et al. (2006) observed increased water absorption in borate-treated wood, which could accelerate biological degradation. Additionally, some studies have highlighted adverse effects on internal bond strength and durability in structural fiberboards treated with fire retardants (Ayrilmis 2007). Ali et al. (2019) found that fire-retardant-treated timber may experience compromised mechanical properties and increased brittleness. The application of these retardants typically requires energy-intensive processes - such as vacuum-assisted impregnation, prolonged drying, and hightemperature curing – which hinder fabrication efficiency and raise environmental concerns. Even bio-based or halogenfree retardants frequently rely on multi-step aqueous treatments, which are inconsistent with the demand for scalable, low-energy, and environmentally sustainable modification techniques (Chen and Wang 2010).

Wood, as a natural composite material with a complex hierarchical structure, has its fire resistance properties significantly influenced by its density and structural complexity (Brando et al. 2012). Densification, particularly when combined with chemical pretreatment, serves as an effective method to enhance wood's fire performance by improving its resistance to ignition and slowing the spread of flames. Kuai et al. (2022) applied chemical pretreatment on poplar wood (Populus tomentosa Carri'ere) to reduce lignin and hemicelluloses, followed by vacuum impregnation with an inorganic sodium silicate solution and high-temperature compressive densification. This combination modification enhanced the mechanical properties, dimensional stability, and fire resistance of the wood composite. Similarly, Zhang et al. (2023) achieved comparable improvements in the properties of poplar through unilateral surface densification after impregnating the wood with waterborne acrylic resin (WAR) and ammonium phytate (APA). The modified wood created by delignification, impregnation, and surface densification of poplar wood exhibited a 3.4-fold increase in strength and a 2.5-fold increase in stiffness compared to untreated wood, along with a 19 % reduction in the peak heat release rate (Peak-HRR) and a 13 % decrease in the peak

smoke production rate (Peak-SPR) compared to untreated wood (Tan et al. 2024). Yue et al. (2020) enhanced the mechanical properties and combustion performance of Chinese fir through densification and impregnation with boric phenol-formaldehyde resin, achieving improved fire performance at higher compression ratios. Wang et al. (2024) applied a boron nitride/graphene oxide composite nanocoating to delignified and densified bamboo, significantly increasing fire resistance by extending ignition time by 67 %. Li et al. (2025) showed that while surface densification improves wood's mechanical properties, flame retardancy, and dimensional stability can be enhanced by introducing ammonium dihydrogen phosphate into the cell walls, although this compromises mechanical properties. The negative effects were mitigated by adding epoxy polymer to the cell cavities. Similar treatments were applied to delignified Chinese fir to produce fire-safe materials (Fan et al. 2023). Chu et al. (2019a, 2019b) achieved fire retardancy in poplar wood through a combination of nitrogen-phosphorus fire retardants and surface thermo-mechanical densification. Özkan et al. (2022) demonstrated that postheat treatment of wood impregnated with fire retardant can potentially make it a reliable engineering material for a wide range of structural applications.

Extensive studies have demonstrated the synergistic effect of chemical modification and densification on improving the fire resistance of wood (Chu et al. 2019a; Gao et al. 2025; Wu et al. 2025; Xu et al. 2023; Zhang et al. 2023). Thermal processing, such as heat treatment or thermal densification, induces surface-core differentiation in wood, forming a multilayered composite structure without the need for external additives (Li et al. 2024; Tang et al. 2025). However, the underlying mechanisms governing the combined influence of chemical treatments and densification on the fire performance of wood remain insufficiently understood - particularly the individual contribution of densification in enhancing fire retardancy.

As sustainability concerns continue to grow, there is an urgent need to explore chemical-free strategies for wood modification (Hasani et al. 2025). Current literature offers limited insights into how thermophysical densification alone affects the combustion behavior of wood. Specifically, the roles of increased surface density and improved structural stability in suppressing fire hazards have not been systematically investigated. Moreover, the mechanistic understanding of how surface-layer alterations induced by densification contribute to fire and smoke suppression is still lacking.

Therefore, this study proposes a chemical-free thermophysical strategy to fabricate surface densified wood and elucidates the underlying mechanisms by which the densified-surface-layer and its structural stability enhance fire and smoke resistance. This approach provides a sustainable and non-toxic route to improve the fire safety of wood, offering valuable insights into the design of environmentally friendly structural materials for advanced engineering applications.

2 Materials and methods

2.1 Materials

Poplar wood (Populus spp.) was selected from Fuyang Forestry Farm, Anhui Province, China. The defect-free and air-dried sapwood was taken from 6 to 7-year-old straight trees at the 1.3-2.3-m section from the bottom. Liquid paraffin (McLean, $\rho = 840-860 \text{ kg/m}^3$, AR) was used to coat the sides of the wood samples; only two surfaces had water exposure.

2.2 Fabrication of the surface densified wood

The air-dried sapwood poplar wood was cut into $120 \times 120 \text{ mm}^2$ (longitudinal × tangential) and at four thicknesses of 14 mm, 15.6 mm, 17.5 mm, and 20.0 mm. The fabrication process and technological parameters of the samples are listed in Table 1 and shown in Figure 1.

The poplar wood samples were first edge-sealed using paraffin, subjected to deionized water impregnation at 20-80 °C, and then kept in a ziplock bag for 2 h to achieve a uniform moisture condition on the surface layer. The densification was carried out using an automatic hot press (PLH-1512, Carver, USA). The up-plate and down-plate reached 160 °C, a wood sample and two steel stoppers with a thickness of 14 mm were placed between the plates, then the pressure rose to 6 MPa with an increased ratio of 20 % and a holding time of 15 min. After that, the heating system turned off, and the pressure was released when the plates' temperature dropped to 60 °C. Then, the surface densified wood samples were removed to a constant-climate chamber under the temperature of 20 °C, relative humidity of 65 % to reach an equilibrium moisture content of 12 %. Then, SDW samples with different compression rates were marked as SDW₂₀-10 %, SDW₂₀-20 %, and SDW₂₀-30 %. SDW samples with different stability were marked as SDW_{no} -30 %, SDW_{20} -30 %, SDW_{50} -30 %, and SDW-30 %. The untreated (control) samples were marked as NW.

To investigate the impact of the densified-surface layer and the non-densified core layers, specimens were produced in which the entire cross-section was densified to the same extent as the surface layers of the surface-densified layer wood (DLW). A density profile tester (X-ray densitometer, CreCon, Martinsried, Germany) was used to determine the density. As shown in Figure 2, samples with a 20, 24, and 28 mm thickness were subjected to deionized water impregnation for 45 min under a pressure of -0.08 MPa and a constant temperature of 80 °C without paraffin edge sealing. After that, they were kept in a microwave at 50 kW for 3 min to achieve a uniform moisture condition in thickness direction. After that, the samples were densified immediately, the densification and conditioning process was the same as the SDW samples. The uniformly densified wood samples were labeled DLW₈₀-30 %, DLW₈₀-40 %, and DLW₈₀-50 %, corresponding to surface densification levels resulting in 30 %, 40 %, and 50 % increases in density compared to untreated poplar wood. The untreated wood, which also represents the non-densified core layer, was called NLW.

2.3 Fire resistance of the surface densified wood

densified wood samples (SDW₂₀-10 %, The surface SDW₂₀-20 %, SDW₂₀-30 %, SDW_{no}-30 %, SDW₅₀-30 %, and SDW₈₀-30 %), uniformly densified wood samples

Table 1: Technological parameters of the SDW samples.

Groups	Impregnation		Densification						
	Temp (°C)	Time (min)	Temp (°C)	Closing speed (%)	Pressure (MPa)	Holding time (min)	Compression ratio (%)		
NW	_	_	_	-	-	-	0		
SDW ₂₀ -10 %	20	30	160	20	6	15	10		
SDW ₂₀ -20 %	20	30	160	20	6	15	20		
SDW ₂₀ -30 %	20	30	160	20	6	15	30		
SDW _{no} -30 %	_	_	160	20	6	15	30		
SDW ₅₀ -30 %	50	30	160	20	6	15	30		
SDW ₈₀ -30 %	80	30	160	20	6	15	30		

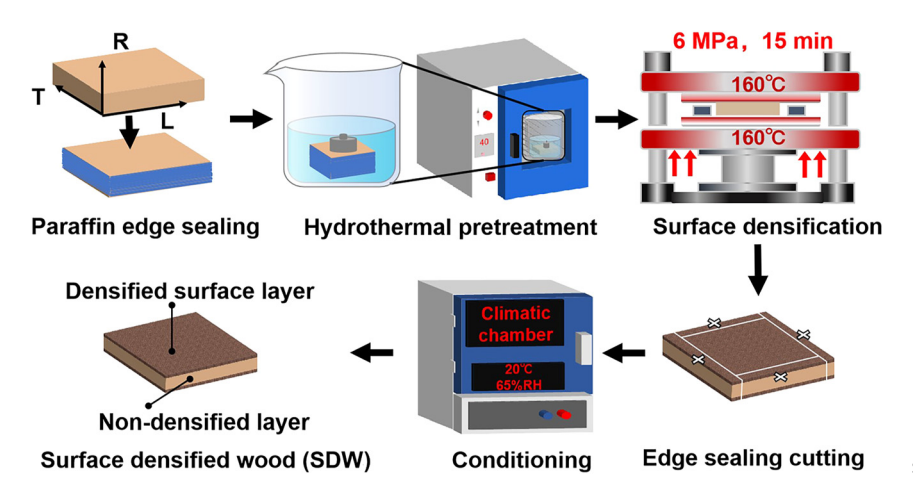


Figure 1: Diagram of fabrication of the SDW samples.

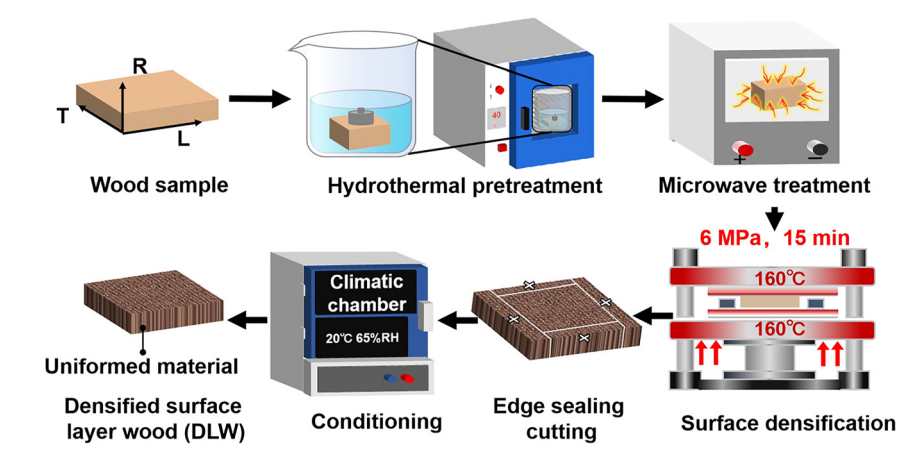


Figure 2: Diagram of fabrication of the uniformly surface densified wood samples.

(DLW $_{80}$ -30 %, DLW $_{80}$ -40 %, and DLW $_{80}$ -50 %), and non-densified layer wood (NLW) were conducted a Cone calorimeter test according to ISO 5660-2002 using a cone calorimeter (Vocho 600, China). The samples with a dimension of $100 \times 100 \times 14 \text{ mm}^3$ (longitudinal \times tangential \times radial) were wrapped with aluminum foil, leaving an 88.4 square surface, then subjected to a 50 kW/m 2 constant external heating flux, which was located 25 mm over the wood surface. Each experimental group consists of three replicates, and the heat and smoke-releasing data were recorded during the samples' combustion process.

DLW₈₀-30 %, DLW₈₀-40 %, and DLW₈₀-50 % were cut into standard specimens for measurement. Samples of $130\times6\times3$ mm³ (longitudinal \times tangential \times radial) underwent limiting oxygen index (*LOI*) according to theGB/T 2406.2–2009 standard, each experimental group consists of 15 replicates. Samples of $25\times25\times6$ mm³ (longitudinal \times tangential \times radial) underwent smoke density rating (*SDR*) according to the GB/T 8627–2007 standard, each experimental group consists of five replicates.

2.4 Moisture-related and heat-related stability of the surface densified wood

Fifteen specimens of each group, including SDW $_{\rm no}$ -30 %, SDW $_{\rm 20}$ -30 %, SDW $_{\rm 50}$ -30 %, and SDW $_{\rm 80}$ -30 %, were kept in a climate chamber with a temperature of 22.5 °C and relative humidity of 65 % for two weeks. The other 15 specimens of each group were put into boiling water for 10 min, then kept for 28 h at room temperature, and oven-dried under 60 °C for 4 h and 103 °C for 8 h. The thickness was measured before and after the humidity and boiling test using a micrometer with an accuracy of 0.001 mm, and the surface hardness was obtained via a Shore D Hardness tester (HS-D, China). The thickness recovery ($T_{\rm RH}$) and hardness recovery ($T_{\rm RH}$) during the humidity test, as well as thickness recovery ($T_{\rm RB}$) and hardness recovery ($T_{\rm RB}$) during the boiling test, were calculated.

$$T_{\rm RH} = \frac{T_{\rm H} - T_{\rm d}}{T_{\rm 0} - T_{\rm d}} \times 100 \,\% \tag{1}$$

$$T_{\rm RB} = \frac{T_{\rm B} - T_{\rm d}}{T_{\rm 0} - T_{\rm d}} \times 100\%$$
 (2)

$$H_{\rm RH} = \frac{H_{\rm H} - H_{\rm d}}{H_0 - H_{\rm d}} \times 100\%$$
 (3)

$$H_{\rm RB} = \frac{H_{\rm B} - H_{\rm d}}{H_0 - H_{\rm d}} \times 100\%$$
 (4)

where T_0 and T_d are the thickness before and after densification, mm; $T_{\rm H}$ is the thickness after the humidity test, mm; $T_{\rm B}$ is the thickness after the boiling test, mm; $H_{\rm 0}$ and $H_{\rm d}$ are the hardness before and after densification; $H_{\rm H}$ is the hardness after the humidity test; $H_{\rm H}$ is the hardness after the boiling test.

A thermal imagery test was also conducted on the $25 \times 25 \times 6$ mm³ (longitudinal × tangential × radial) samples using a self-made device, which consists of a digitally displayed electric furnace (FL-2A, Mingjie Instrument., China) and a thermal imaging system (HM-TPH10S-3AQF, China) 200 mm over the furnace surface. Each experimental group consists of three replicates. Samples were put in the furnace when the surface temperature was maintained at 160 °C. The temperature changes of the samples were recorded.

2.5 Morphological and chemical analysis of the surface densified wood

In order to uncover the deformation stability of the surface densified wood, morphological changes of wood cell wall of the densified surface layer part before and after the boiling test, as well as after combustion were investigated via scanning electron microscopy (SEM Sirion 200, FEI, USA). All samples were gold-coated prior to being placed inside the SEM specimen chamber.

The NLW and DLW₈₀-50 % samples were grounded into 200-mesh powder and oven-dried. Five mg of the powder sample was tested using a thermogravimetric analyzer (TGA, Q600, TA Instruments, USA). Each experimental group consists of three replicates. Nitrogen was used as shielding gas, and the temperature increased by 10 °C/min. Fourier transform infrared (FTIR) spectroscopy was carried out on an FTIR spectrometer (TENSOR II, BRUKER, Germany) with a wavenumber range from 4,000 to 400 cm⁻¹, resolution of 8 cm⁻¹, and a frequency of 32 times. A polycrystalline X-ray diffractometer (XRD-6, Beijing Spectrometer) was used to analyze and calculate the degree of crystallinity, with an instrument operating voltage of 36 kV, a current of 20 mA, and a scanning range of 2θ = 5° to 70° at a scanning speed of 4°/min.

3 Results and discussion

3.1 Effect of the densification intensity on the fire resistance of SDW

Combustion parameters of the SDW samples with the compression rate of 10 %, 20 %, and 30 % were listed in Table 2. The density distribution, heat, and gas-releasing properties are displayed in Figure 3.

As shown in Table 2, the TTI, Time-HRR₁, Time-HRR₂, and Time-70 % mass loss of the SDW samples were prolonged, and Peak-HRR1 and Peak-HRR2 values were reduced when compared to the NW. During the first 360 s of combustion, 'NW's THR was 68.2 MJ m^{-2} , and SDW_{20} -10 %, SDW_{20} -20 %and SDW₂₀-30 % decreased by 19.1 %, 21.4 %, and 20.2 %. The 70 % mass of the NW was burned out in 373 s, while it caused an extra 36 s, the 70 s, and 171 s for the SDW₂₀-10 %, SDW₂₀-20 %, and SDW₂₀-30 % wood. The densified surface layer delayed the thermal degradation reaction and alleviated the intensity of wood combustion.

According to Figure 3a, the SDW samples display a sandwich structure, with two DL and one NL. The density of SDW₂₀-10 % ranges from 400 to 710 kg/m³, with an average value of 490 kg/m³, exhibiting two DL with a thickness of 2.5 mm. As the compression ratio increases, the average densities of the SDW₂₀-20 % and SDW₂₀-30 % samples reach 540 kg/m³ and 620 kg/m³, respectively, while the DL's thickness increases to 4 and 5.5 mm.

Table 2: Cone test parameters of the SDW samples with different compression rates.

Item	Groups						
	NW	SDW ₂₀ -10 %	SDW ₂₀ -20 %	SDW ₂₀ -30 %			
TTI (s)	13	14	16	19			
Peak-HRR ₁ (kW m ⁻²)	303.9	255.8	255.1	247.3			
$Peak-HRR_2$ (kW m $^{-2}$)	360.8	238.6	244.8	294.1			
$Time-HRR_1$ (s)	49	53	35	60			
Time- HRR_2 (s)	378	411	445	554			
Time-70 % mass loss (s)	372	408	442	543			
HRR (kW m ⁻²)	93.3	84.8	79.5	96.4			
HRR_{360} (kW m ⁻²)	330.4	173.8	136.5	132.8			
THR (MJ m ⁻²)	142.3	134.455.2	127.2	453.6			
THR_{360} (MJ m ⁻²)	68.2	55.2	53.6	54.4			
TSP (m ²)	2.0	1.9	1.7	2.3			
$TSP_{360} (m^2)$	1.4	0.9	0.9	0.4			
COY (kg/kg)	0.45	0.33	0.33	0.22			
CO_2Y (kg/kg)	4.83	4.62	4.33	3.83			

TTI refers time to ignition, HRR refers to heat release rate, THR refers to total heat release, TSP refers to total smoke production, COY refers to CO yield, CO₂Y refers to CO₂ yield. HRR₃₆₀, THR₃₆₀, and TSP₃₆₀ refer to mean value of HRR, THR, and TSP in the first 360 s.

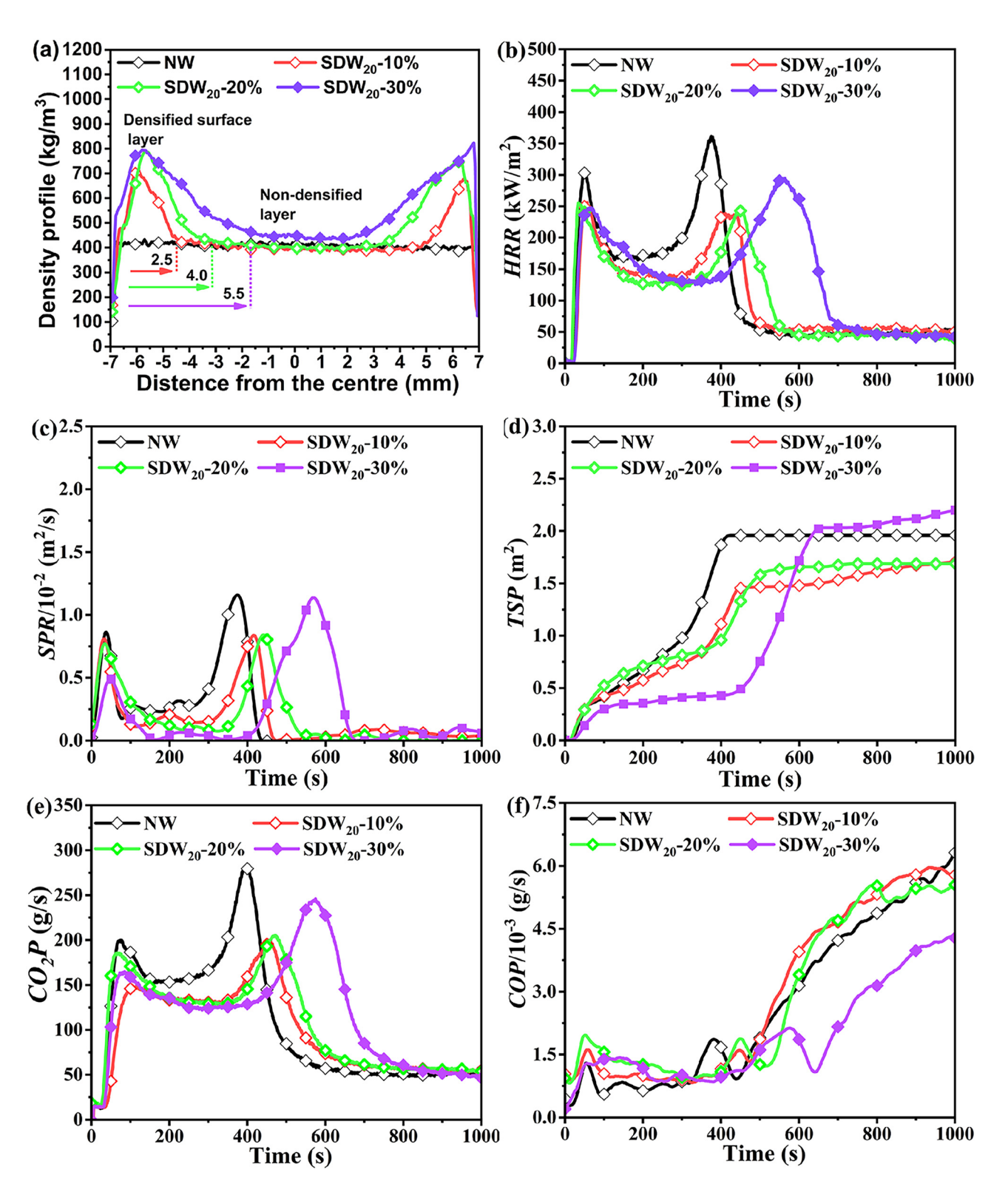


Figure 3: Density profile (a), heat release rate (b), smoke production rate (c), total heat release (d), CO₂ production rate (e), and CO production rate (f) of the SDW samples with different compression rates.

The HRR curve of both NW and SDW samples exhibit two peaks (Figure 3b). The ignition and early combustion phases of wood generate highly flammable gases such as carbon monoxide, methane, and other hydrocarbons, which contribute to the rapid increase in HRR (Lai et al. 2024). Meanwhile, the wood surface is subjected to heat and transformed into charcoal, which releases less energy than that of volatile gases. However, the internal wood layers release new volatile gases, leading to a second increase in heat release when the surface charcoal burns out or cracks, allowing heat from the fire to reach deeper layers of the wood. Therefore, the formation and thermal stability of the surface charcoal are essential to the fire resistance property of wood.

The HRR curve of the SDW after Peak-HRR1 (before Peak-HRR2) is much lower than that of NW. Time-HRR2 of SDW increased significantly with the compression ratio, resulting in 33 s, 67 s, and 176 s delay compared with NW. Furthermore, the Peak-HRR2 values declined from 238.6 kW m⁻², 360.8 kW m^{-2} to 244.8 kW m^{-2} 294.1 kW m⁻². It can be inferred that the formation of a thicker and more stable charcoal layer on the SDW sample's surface slowed down heat transfer and the spread of the flame, thus extending the Time-HRR2. The overall shift of the CO_2P curves to the right could also prove it (Figure 3e).

Figure 3c, d and f display SDW samples' smoke and CO release. Like HRR curves, SDW samples' SPR and COP curves shifted to the right as the compression ratio increased. Significant smoke suppression enhancement could be found for the SDW samples, especially during the first 600 s. Considering the weight, the SDW sample possesses 10-30 % higher mass than NW, while the TSP of SDW_{20} -10 % and SDW_{20} -20 % was 5.1% and 13.8% lower. Even for the SDW₂₀-30% wood, its TSP and COP curves were lower than NW.

3.2 Effect of deformation stability on the fire resistance of SDW

Table 3 shows the heat and smoke-release-related parameters of SDW samples with different deformation stability in the CONE test. Figure 4 presents the HRR, THR, SPR, TSP, CO₂ production yield (CO_2Y) , and CO production yield (COY)curves. The deformation recovery rate can reflect the stability of the SDW samples during moisture absorption and boiling treatments. The test results for the surface hardness and radial thickness recovery rate of the SDW samples before and after boiling and moisture absorption, as well as SEM images, are shown in Figure 5.

As illustrated in Figure 4a, the Peak-HRR₁ of the SDW samples decreased, and the occurrence of Time-HRR2 was

Table 3: Heat and smoke release of the SDW samples with different deformation stability.

Item	Groups						
	SDW _{no} - 30 %	SDW20- 30 %	SDW ₅₀ - 30 %	SDW ₈₀ - 30 %			
TTI (s)	16	19	20	20			
Peak-HRR ₁	320.5	247.3	222.3	189.2			
$(kW m^{-2})$							
Peak-HRR ₂	415.9	294.1	308.3	341.9			
$(kW m^{-2})$							
$Time-HRR_1$ (s)	42	60	48	46			
Time-HRR $_2$ (s)	428	554	579	627			
THR_{600} (MJ m ⁻²)	114.8	103.5	89.6	76.3			
THR (MJ m ⁻²)	171.8	153.6	145.6	131.6			
COY (kg/kg)	0.42	0.22	0.15	0.15			
CO_2Y (kg/kg)	5.64	3.83	3.65	3.43			
$TSP_{600} (m^2)$	2.2	1.7	1.4	1.0			
TSP (m ²)	2.2	2.3	2.1	1.8			

HRR₆₀₀, THR₆₀₀, and TSP₆₀₀ refer to mean value of HRR, THR, and TSP in the

delayed as the deformation stability of the densified surface layer increased. Compared to SDW $_{no}$ -30 % wood, the Time-HRR₂ of the SDW₂₀-30 %, SDW₅₀-30 %, and SDW₈₀-30 % wood was extended by 126 s, 151 s, and 199 s, respectively. These results suggest that enhanced densified surface layer stability promotes the formation of a denser and more robust char layer during combustion, which is less prone to rupture and more effective at impeding heat transfer. After 700 s, the HRR curves stabilized, reflecting the heat release from residual char ablation. Notably, the HRR values of the SDW samples remained significantly lower, indicating that improved densified surface layer stability also facilitated the transformation of the inner wood into thermally stable char with superior thermal insulation and oxygen barrier properties. As shown in Figure 4b, enhanced deformation stability of the densified layer effectively suppressed heat release throughout the combustion process.

As shown in Figure 4d-f, the SPR, TSP, and COY curves of the SDW samples significantly declined, indicating that the char layer formed during the combustion phase of wood blocks heat transfer and effectively suppresses smoke generation. The SDW samples' TSP values decrease with the increase in deformation stability. For instance, SDW₈₀-30 % wood's TSP value is 1.43 m², a reduction of 35.9 % compared to SDW_{no}-30 % wood within the 1,000 s of combustion. The average COY and CO2Y values of the SDW samples are significantly lower, especially within the first 600 s of combustion, where the average COY and CO_2Y of the SDW samples are almost zero, indicating that the better the stability of the DL, the stronger the protective capability of the char

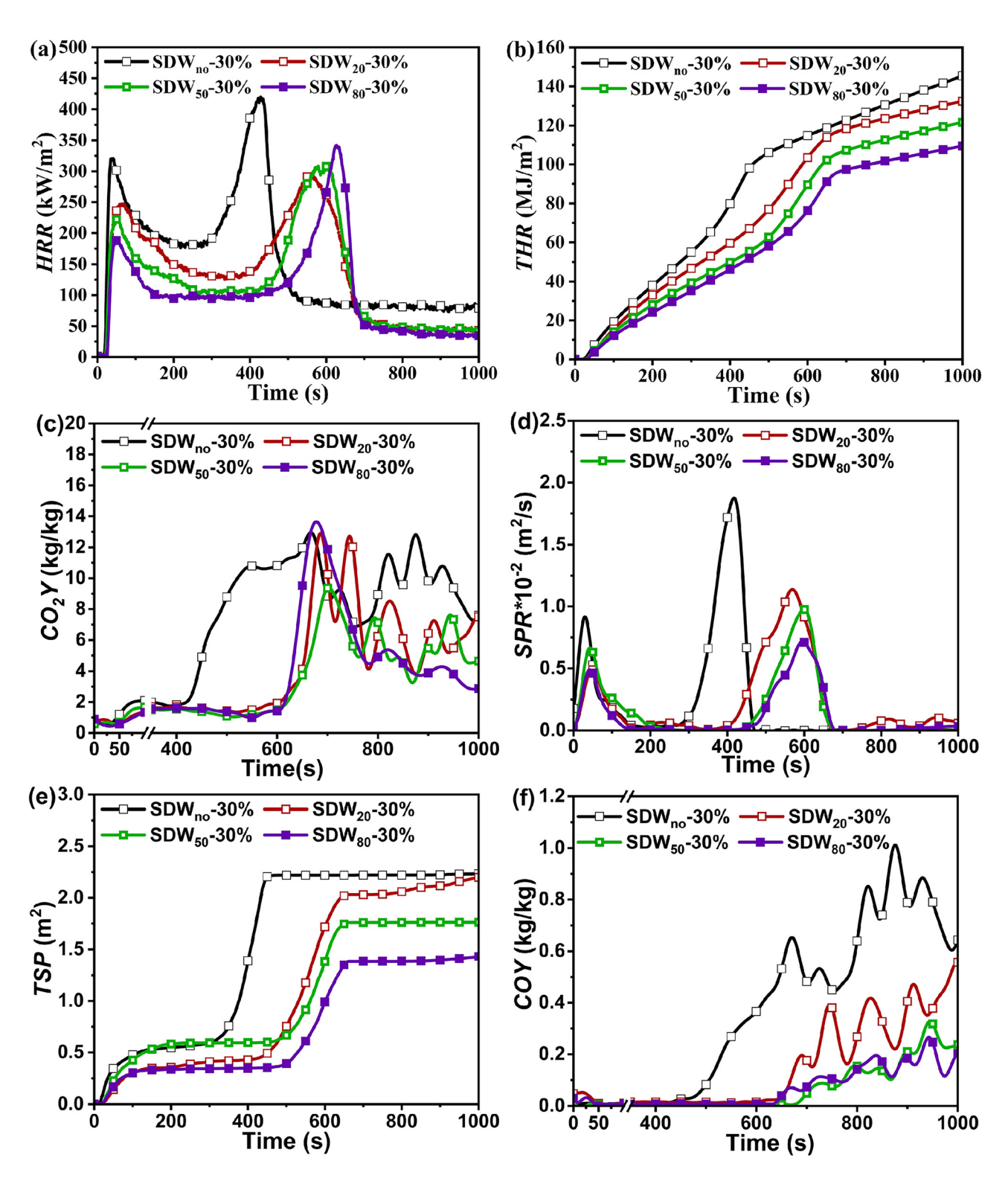


Figure 4: Heat release rate (a) and total heat release (b), CO₂ production yield (c), smoke production rate (d), total smoke production (e), and CO production yield (f) of the SDW samples with different deformation stability.

layer formed during combustion. Consequently, the production of smoke and the generation of CO and CO₂ are significantly reduced. Reducing CO and CO₂ generation is critical for mitigating casualties caused by toxic gases.

As shown in Figure 5a and b, the SDW samples' boiling and humidity hardness and thickness recovery decreased with increasing hydrothermal pretreatment temperature. SDW $_{\rm no}$ -30 % wood did not undergo the pretreatment and had

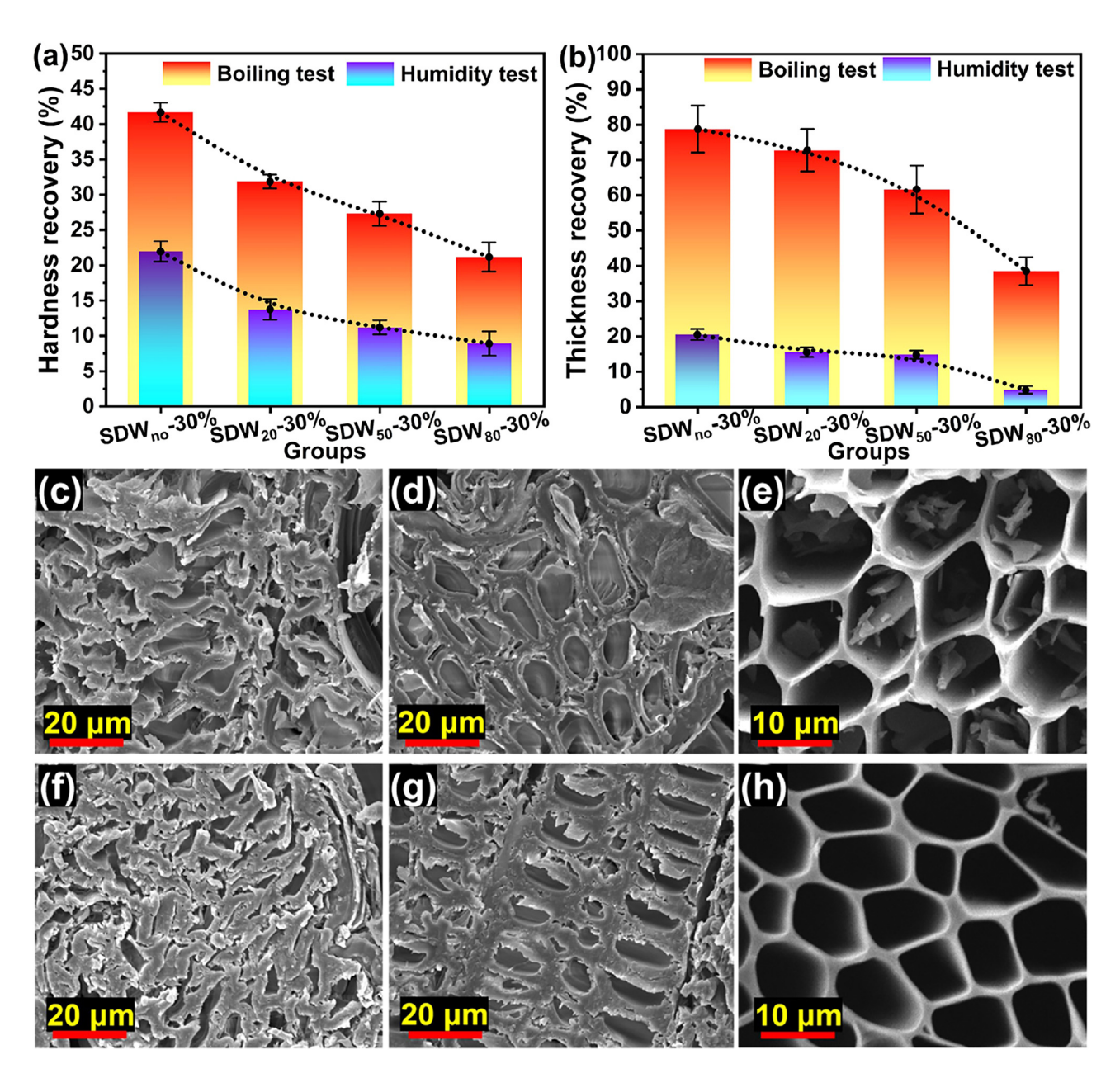


Figure 5: Hardness recovery (a), thickness recovery (b), SEM images of SDW₂₀-30 % (c), SDW₈₀-30 % (f) after densification, SEM images of SDW₂₀-30 % (d), SDW₈₀-30 % (g) after boiling test, SEM images of SDW₂₀-30 % (e), SDW₈₀-30 % (h) charcoal after combustion.

a boiling thickness recovery rate and humidity thickness recovery rate of $78.8\,\%$ and $20.7\,\%$, respectively. For the SDW₈₀-30 % wood, the boiling and humidity thickness recovery rates were only $38.5\,\%$ and $5.0\,\%$, showing a decrease of $40.3\,\%$ and $15.7\,\%$. The hydrothermal pretreatment significantly improved the stability of the densified poplar wood composites in humid/water environments (Wang et al. 2012).

Based on the morphological analysis of SDW samples after densification shown in Figure 5c and f, it could be found that the SDW $_{20}$ -30 % wood cell wall severely cracked, and the

80 °C hydrothermal pretreatment mitigated it. Fewer gaps were found in the cross-section of SDW₈₀-30 % wood. After the boiling test, the SDW₈₀-30 % cell wall maintained the deformation mostly, while the SDW₂₀-30 % wood had a severe recovery. After combustion, most of the densified surface layer material was consumed; however, as shown in Figure 5e and h, the charred center layer of SDW₈₀-30 % wood exhibited significantly thickened cell walls, indicating that a more stable densified surface layer provides improved protection of the inner wood structure against thermal degradation.

3.3 Mechanistic insights into the fireretardant effect of densified surface layer in SDW samples

3.3.1 Difference in combustion process of densified surface layer wood and non-densified layer wood

The difference in LOI, SDR, and heat and smoke releasing of the non-densified layer wood (NLW) and densified surface layer wood (DLW) samples was illustrated in Figure 6.

The DLW sample's LOI was higher than NLW, revealing that the densified surface layer enhanced the ignition performance of the SDW samples. As the density increased, the SDR of the DLW rose sharply. It could be explained by the incomplete combustion of highly compressed wood, which can produce more smoke. Meanwhile, the DLW sample's residual weight increased largely from 2.5 % to 17.0 %, proving that the densified surface layer in SDW could transform into a more dense and stable charcoal.

For heat release during the CONE test, it was found that the DLW sample's HRR curve moved right as the density increased. The Time-HRR2 delayed 200 s, 300 s, and 400 s for DLW₈₀-30 %, DLW₈₀-40 %, and DLW₈₀-50 % wood. Similarly, the SPR curves moved right and decreased. The THR of DLW samples were higher than NLW because their density and weight were 30-50 % higher (Figure 6d). However, DLW samples' TSP declined significantly, with the peak delayed from 360 s to 960 s. Regarding toxic gas, the CO production rate of DLW samples was much lower than that of NLW during combustion. Therefore, these results prove that the densified surface layer played an important role in reducing heat and smoke release in the SDW samples during the combustion.

To further investigate the barrier effect of the densified surface layer on the combustion of the SDW samples during the CONE test, the correlation between the HRR, SPR and the specific mass loss (SMLR), fire performance index (FPI), and fire growth index (FGI) of the SDW, DLW, and NLW samples were calculated based on CONE data.

According to Figure 7 and Table 4, the fitting slope of the HRR/SMLR on SDW samples increased slightly with the densification intensity of the densified surface layer while decreasing largely with densified surface layer's deformation stability, SDW_{no} -30 % > SDW_{20} -30 % > SDW_{50} -30 % > SDW_{80} -30 %. For the fitting slope of the SPR/SMLR, the value increased with the densification intensity of densified surface layer and decreased with the densified surface layer deformation stability. Therefore, the deformation stability of the densified surface layer played an important role both in enhancing the fire resistance and suppressing the smoke release of the SDW samples.

Compared with the NLW sample, the fitting slope of the HRR/SMLR and SPR/SMLR on DLW samples (except DLW₈₀-30 %) were decreased, uncovering that the densified surface layer part of the material in the SDW samples was better in both fire resistance and smoke suppression than the corelayer material. Furthermore, the fitting slope of the HRR/ SMLR for the SDW₈₀-30 % sample was significantly lower than those of both NLW and DLW, implying that interactions occur between the densified surface layer and non-densified core layer during combustion, thereby enhancing the overall fire performance of the SDW samples. The densified surface layer acts as an effective, chemical-free fire barrier that can transform into a more stable char layer, reducing combustion intensity and toxic gas emissions. Sandwich structuring densification has proven to be a sustainable strategy for enhancing the fire safety of wood, offering valuable insights into developing safer, bio-based materials for fire-prone environments. However, the combustion interactions between the densified surface layer and the non-densified core layer warrant further investigation.

3.3.2 Difference in chemistry and morphology of the densified surface layer wood and non-densified layer wood

The SDW sample is a composite material consisting of both densified and non-densified parts. Therefore, to analyze the mechanism by which the densified surface layer contributes to the flame retardant performance of the SDW samples, it is essential to conduct separate analyses of the densified surface layer and non-densified layer materials. Figure 8 presents the characterization of DLW and NLW using density profiling, TG, thermal conductivity measurement, XRD for crystallinity, and FTIR for chemical structure analysis.

Figure 8a shows that the density distribution of the DLW samples is relatively uniform along the thickness direction, particularly in the DLW₈₀-50 % sample. The average densities of DLW $_{80}$ -30 %, DLW $_{80}$ -40 %, and DLW $_{80}$ -50 % are approximately 630 kg/m³, 750 kg/m³, and 900 kg/ m³, respectively, which are comparable to the surface-layer densities of the SDW20-10 % to SDW20-30 % samples discussed above. Therefore, the DLW₈₀-30 % to DLW₈₀-50 % samples represent the densified surface layer in the surface densified wood.

Figure 8b illustrates the infrared spectroscopy; the characteristic absorption bands of the DLW samples are similar to those of the NLW, with differences only in the peak intensities. Hygroscopic components such as hemicellulose of DLW samples undergo degradation, causing cellulose chains to rearrange and an increase in the relative content of lignin (Luo et al. 2024). The absorption peak at 3,340 cm⁻¹,

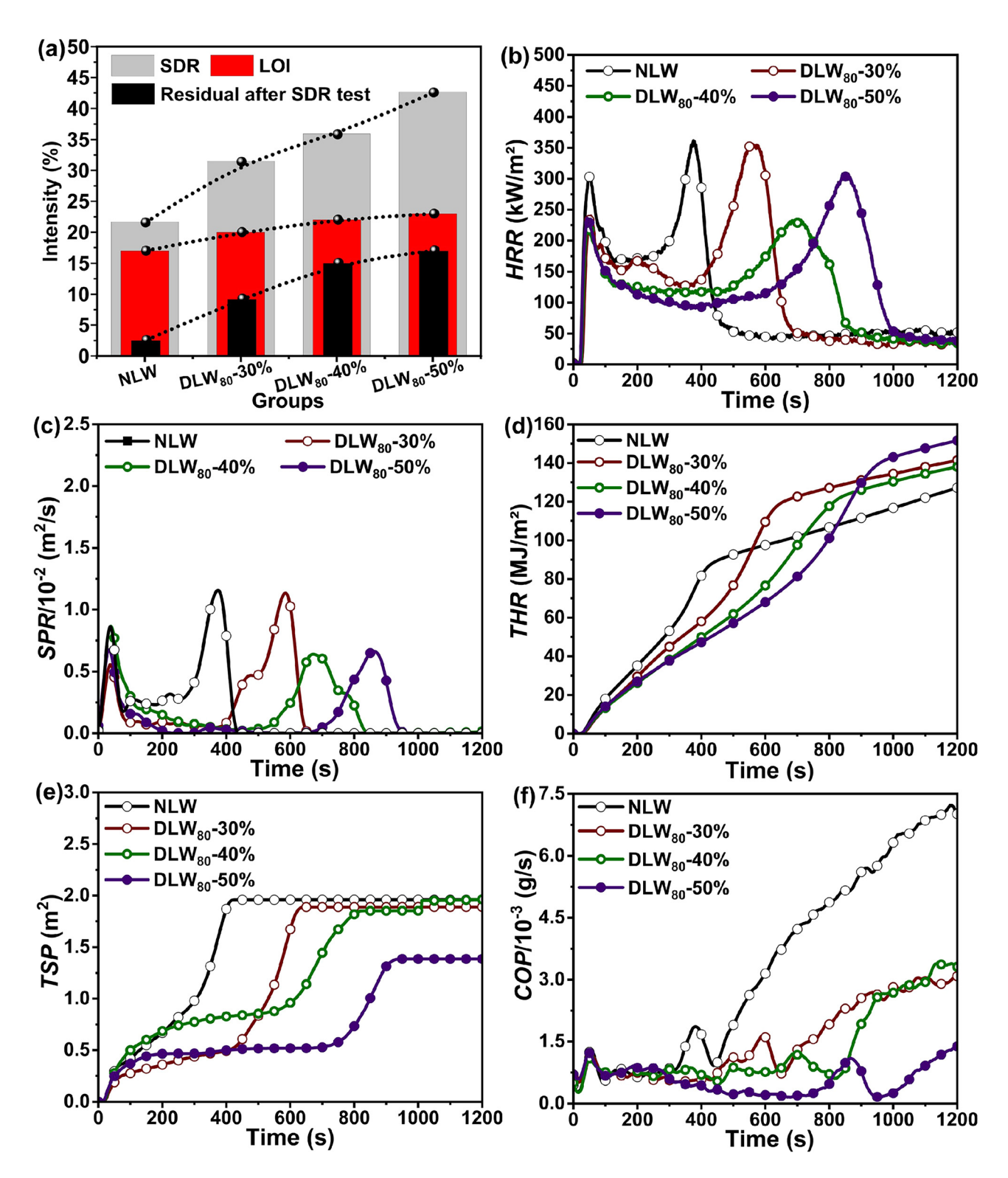


Figure 6: LOI and SDR (a), heat release rate (b), smoke production rate (c), total heat release (d), total smoke production (e), and CO production rate (f) of the DLW and NLW samples.

associated with the stretching vibration of hydroxyl groups (–OH) in wood, shows a decrease in intensity. Conversely, the absorption peak at 1732 cm⁻¹, corresponding to the

stretching vibration of carbonyl groups (C=O), gradually increases in intensity. The characteristic peak at 2,902 cm⁻¹, related to the stretching vibration of C–H bonds, also

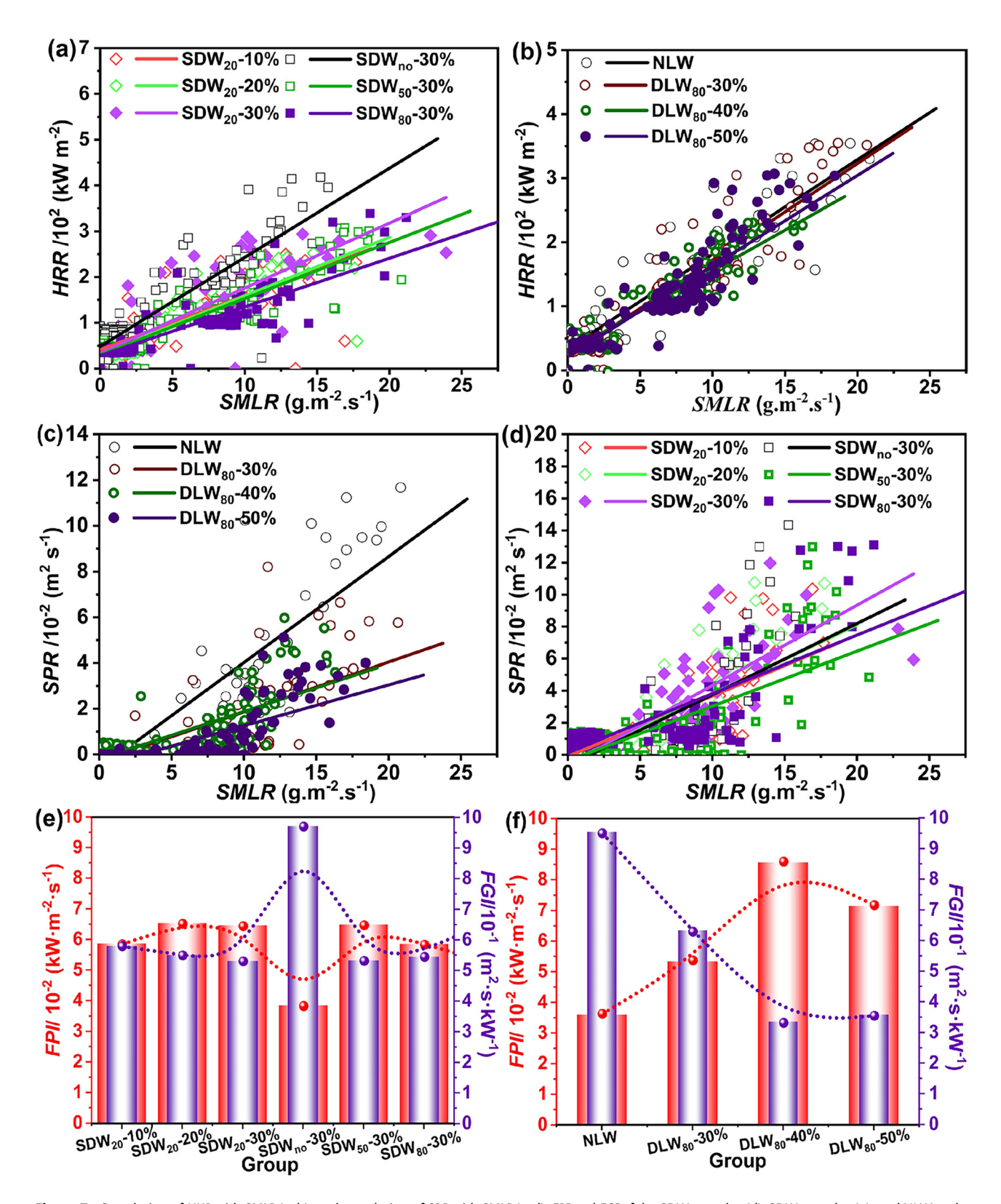


Figure 7: Correlation of *HHR* with *SMLR* (a, b), and correlation of *SPR* with *SMLR* (c, d), *FPI* and *FGI* of the SDW samples (d), SDW samples (e), and NLW and DLW samples (f).

Table 4: The linear statistical dependence of the *HHR* and *SPR* on the specific mass loss rate.

Groups	HRR/SMLR		SPR/SMLR		Group	HRR/SMLR		SPR/SMLR	
	Slope	R ²	Slope*E ⁻⁴	R ²		Slope	R ²	Slope*E ⁻⁴	R ²
SDW ₂₀ -10 %	11.6	0.83	3.8	0.77	SDW ₈₀ -30 %	10.6	0.86	3.7	0.73
SDW ₂₀ -20 %	12.8	0.90	4.3	0.83	DLW ₈₀ -30 %	15.1	0.94	3.4	0.74
SDW ₂₀ -30 %	14.2	0.87	5.0	0.87	DLW ₈₀ -40 %	12.7	0.90	3.2	0.71
SDW _{no} -30 %	19.5	0.91	4.4	0.71	DLW ₈₀ -50 %	14.1	0.91	2.8	0.71
SDW ₅₀ -30 %	12.3	0.91	3.4	0.72	NLW	14.8	0.95	4.6	0.88

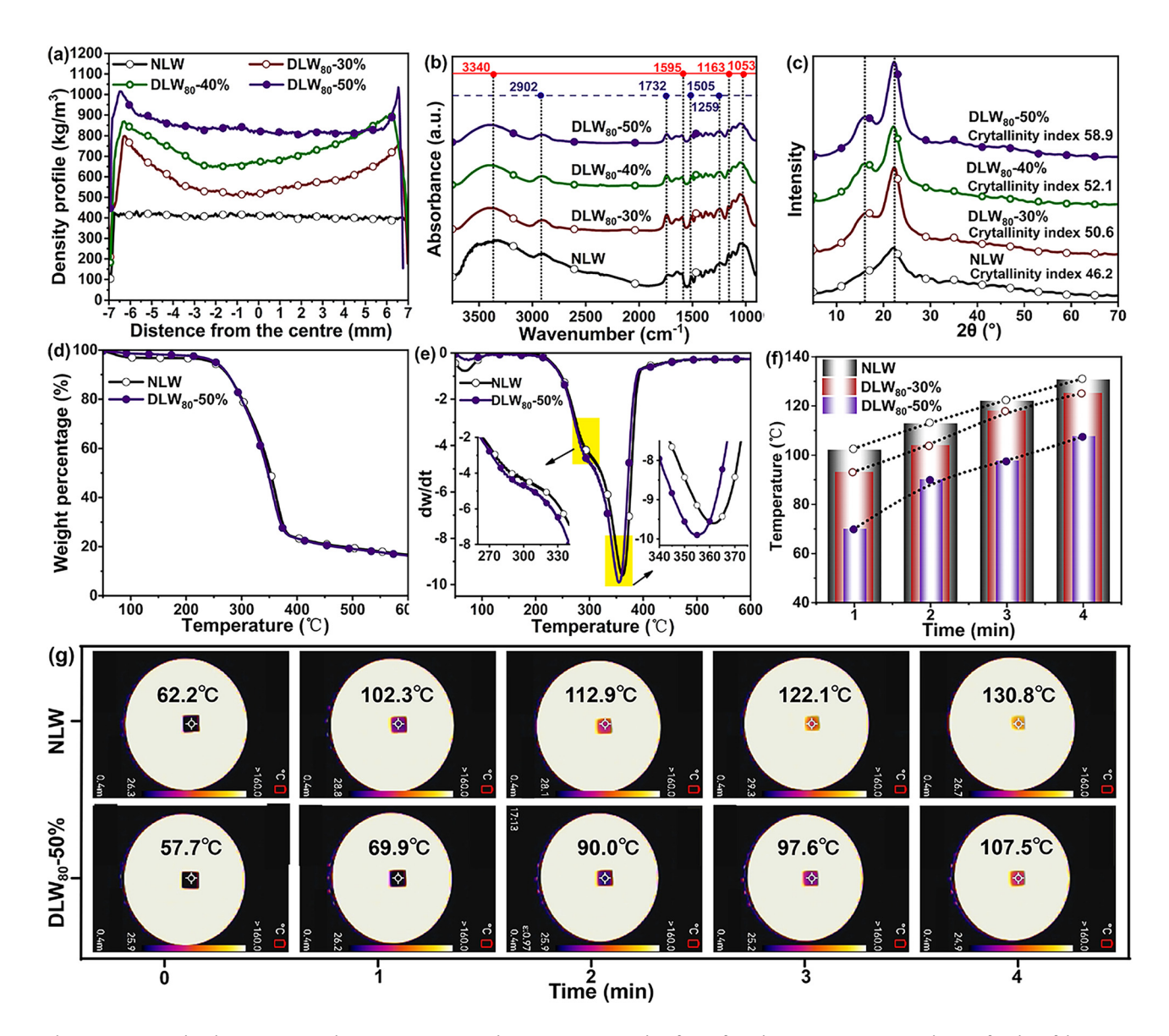


Figure 8: Density distribution (a), FT-IR (b), XRD (c), TG curves (d), DTG curves (e), and surface infrared imaging temperature change (f and g) of the DLW and NLW samples.

intensifies, indicating the rupture and reorganization of hydrogen bonds, which may result in a relative increase in methylene group functionality. The absorption peaks around 1,595 cm⁻¹ and 1,505 cm⁻¹ intensify, and the C-O-C stretching vibration peak at 1,259 cm⁻¹ also increases, all suggesting an increase in the relative content of lignin. Under heat and pressure, hemicelluloses undergo partial degradation, increasing the proportion of crystalline cellulose regions. The amorphous region of cellulose experiences cross-linking, resulting in a more orderly arrangement of microfibrils, reducing the intermolecular distance and promoting the formation of new hydrogen bonds (Tang et al. 2019). The stability of the lignin aromatic ring structure is relatively high, and the increased absorption peak corresponding to the aromatic ring skeleton indicates an enhancement in the thermal stability of poplar wood. The intensity of the C-H bending vibration absorption peak at 1,374 cm⁻¹, the C-O-C stretching vibration absorption peak at 1,163 cm⁻¹, and the C-O stretching vibration absorption peak at 1,053 cm⁻¹ decreased, likely due to the thermal decomposition or cleavage of less stable polysaccharide components, such as hemicellulose, under high-temperature heat treatment, leading to a reduction in the content of cellulose and hemicellulose (Wang et al. 2021). As shown in Figure 8e, the DLW samples' crystallinity is higher than that of the NLW, wherein the DLW₈₀-50 % sample's crystallinity reaches up to 58.9 %.

As shown in Figure 8d and e, the thermal stability of the DLW80-50 % is slightly enhanced compared to that of NLW. In the first degradation stage (30-210 °C), the weight loss of the NLW sample is mainly attributed to the evaporation of adsorbed water and the partial decomposition of hemicellulose (Yang et al. 2007). In contrast, DLW₈₀-50 % retains a higher mass fraction during this stage, indicating greater resistance to early thermal decomposition, which may be related to increased crystallinity (Figure 8c). During the rapid pyrolysis phase, the decomposition temperature range of DLW₈₀-50 % shifts leftward to 210-356 °C, with the peak weight loss temperature reduced by 22 °C compared to NLW. Meanwhile, the maximum weight loss rate is higher, suggesting that DLW_{80} -50 % transitions into the carbonization phase more rapidly.

Interestingly, the final char residue of the DLW₈₀-50 % sample shows minimal change (Figure 8d), indicating that densification does not significantly improve the overall thermal stability of poplar wood through chemical composition modification. Meanwhile, a significant temperature difference is observed at the center of the DLW80-50 % sample and NLW sample during the early heating stage (Figure 8f and g), indicating that the densified surface layer of the surface densified wood, due to its higher density and denser charcoal, exhibits greater resistance to heat conduction. This phenomenon can be attributed to the denser internal fiber structure, which extends the thermal conduction path and slows heat transfer. Moreover, the densified surface layer has a higher heat capacity, requiring more energy to raise its temperature (Zhou et al. 2024). As heating progresses, the temperature difference gradually decreases, implying that the influence of density on thermal conductivity weakens over time.

Therefore, the enhanced flame-retardant performance of the surface densified wood is primarily ascribed to the earlier formation of a protective char layer. The observed improvements in thermal stability can be attributed to the early decomposition of hemicellulose and the consequent increase in the proportion of lignin, which plays a crucial role in char formation (Soula et al. 2024). This char layer serves as an effective physical barrier, significantly reducing heat release and smoke generation compared to untreated wood.

4 Conclusions

In this study, surface densified wood with different densification degrees and deformation stability were fabricated, providing a chemical-free approach to improving wood fire safety. Additionally, it thoroughly examined the impact of the surface densified layer on fire and smoke suppression properties of the wood. The main findings are as follows:

- The surface densified wood fabricated is a functional material, consisting of densified surface layer and nondensified layer with distinct structural and compositional characteristics.
- 2) The densified surface layer acts as an effective thermal and combustion barrier, delaying ignition, reducing peak heat release rates, and suppressing smoke and toxic gas emissions. Compared with untreated wood, the ignition time of SDW₂₀-30 % prolonged 46 %, time to heat release peak delayed 176 s, and CO yield declined 51 %.
- 3) The deformation stability of the densified surface layer – optimized through hydrothermal pretreatment - was found to have a greater influence on sustained fire resistance than densification degree alone. Compared with SDW₂₀-30 %, the time to heat release peak of SDW₈₀-30 % prolonged 73 s, and total heat and smoke release further declined 14 % and 22 %.
- 4) Thermal, chemical, and morphological analyses confirmed that densification increased cellulose crystallinity, modified chemical composition, and promoted the formation of a stable char layer, thereby enhancing the thermal shielding effect and protecting the nondensified layer during combustion. The improved deformation stability of surface-densified wood contributes to a more stable and efficient char barrier, thereby enhancing heat and smoke suppression.

This chemical-free approach offers a promising strategy for developing fire-resistant wood. Yet, the long-term performance under repeated environmental stresses – including UV exposure and wet-dry cycles – as well as the precise control of the densified layer's thickness and deformation stability, remain critical challenges that need further exploration for real-world use. Future research should also explore its scalability, applicability to other diverse wood species, and integration with multifunctional treatments.

Research ethics: Not applicable. Informed consent: Not applicable.

Author contributions: Writing – original draft preparation: D.C., X.R., Y.Z., S.R., V.N.; formal analysis: D.C.; investigation: X.R., Z.Y.; resources: D.C.; S.L. conceptualization: D.C., methodology: D.C., supervision: D.C.; A.S.; S.L; writing - review and editing: A.S.; D.C. The authors have accepted responsibility for the entire content of this manuscript and approved its submission.

Use of Large Language Models, AI and Machine Learning **Tools:** None declared.

Conflict of interest: The authors state no conflict of interest. **Research funding:** This work was financially supported by the National Natural Science Foundation of China (no. 32401503); China Scholarship Council Program (no. 202308340065) for visiting scholar work in the University of British Columbia.

Data availability: Not applicable.

References

- Ahn, N., Dodoo, A., Riggio, M., Muszynski, L., Schimleck, L., and Puettmann, M. (2022). Circular economy in mass timber construction: state-of-theart, gaps and pressing research needs. J. Build. Eng. 53: 104562.
- Ali, S., Hussain, S.A., and Tohir, M.Z.M. (2019). Fire test and effects of fire retardant on the natural ability of timber: a review. Pertanika J. Sci. Technol. 27: 867-895.
- Ayanleye, S., Udele, K., Nasir, V., Zhang, X., and Militz, H. (2022). Durability and protection of mass timber structures: a review. J. Build. Eng. 46:
- Ayrilmis, N. (2007). Effect of fire retardants on internal bond strength and bond durability of structural fiberboard. Build. Environ. 42: 1200-1206.
- Baysal, E., Sonmez, A., Colak, M., and Toker, H. (2006). Amount of leachant and water absorption levels of wood treated with borates and water repellents. Bioresour. Technol. 97: 2271-2279.
- Brando, P.M., Nepstad, D.C., Balch, J.K., Bolker, B., Christman, M.C., Coe, M., and Putz, F.E. (2012). Fire-induced tree mortality in a neotropical forest: the roles of bark traits, tree size, wood density and fire behavior. Glob. Chang. Biol. 18: 630-641.
- Chen, G.G., Chen, C.J., Pei, Y., He, S.M., Liu, Y., Jiang, B., Jiao, M.L., Gan, W.T., Liu, D.P., Yang, B., et al (2020). A strong, flame-retardant, and thermally insulating wood laminate. Chem. Eng. J. 383: 123109.

- Chen, L. and Wang, Y.Z. (2010). A review on flame retardant technology in China. Part I: development of flame retardants. Polym. Advan. Technol. 21: 1-26.
- Chu, D.M., Mu, J., Avramidis, S., Rahimi, S., Liu, S.Q., and Lai, Z.Y. (2019a). Functionalized surface layer on poplar wood fabricated by fire retardant and thermal densification. Part 1: compression recovery and flammability. Forests 10: 955.
- Chu, D.M., Mu, J., Avramidis, S., Rahimi, S., Liu, S.Q., and Lai, Z.Y. (2019b). Functionalized surface layer on poplar wood fabricated by fire retardant and thermal densification. Part 2: dynamic wettability and bonding strength. Forests 10: 982.
- Dasari, A., Yu, Z.Z., Cai, G.P., and Mai, Y.W. (2013). Recent developments in the fire retardancy of polymeric materials. Prog. Polym. Sci. 38: 1357-1387.
- Fan, C.G., Gao, Y.X., Li, Y.H., Yan, L., Zhu, D.J., Guo, S.C., Ou, C.H., and Wang, Z. (2023). A flame-retardant densified wood as robust and fire-safe structural material. Wood Sci. Technol. 57: 111-134.
- Gao, X.D., Gong, R.Z., Hu, X.J., Gu, Y.S., Srinivasan, V., Dong, X.Y., and Li, Y.F. (2025). Highly strong, fire-retardant and water-resistant wooden structural material enabled by organic-inorganic nanohybridization in-situ coupled with cell densification. Chem. Eng. J. 515: 1080-1093, 1385-8947.
- Goubran, S., Masson, T., and Walker, T. (2020). Diagnosing the local suitability of high-rise timber construction. Chem. Eng. J. 48: 101-123.
- Harada, T., Nakashima, Y., and Anazawa, Y. (2007). The effect of ceramic coating of fire-retardant wood on combustibility and weatherability. J. Wood Sci. 53: 249-254.
- Hasani, N., Hosseini, A., Ashjazadeh, Y., Diederichs, V., Ghotb, S., Riggio, M., Nasir, M.V., and Nasir, V. (2025). Outlook on human-centred design in industry 5.0: towards mass customisation, personalisation, co-creation, and co-production. Int. J. Sustain. Eng. 18: 2486343.
- Huang, Y.X., Lin, Q.Q., Fu, F., Lin, L.Y., and Yu, W.J. (2023). Scalable highperformance wood-based composites prepared by hydro-mechanical treatment. Compos. B Eng. 267: 111041.
- Kuai, B., Wang, Z., Gao, J., Tong, J., Zhan, T., Zhang, Y., Lu, J., and Cai, L. (2022). Development of densified wood with high strength and excellent dimensional stability by impregnating delignified poplar by sodium silicate. Constr. Build. Mater. 344: 128282.
- Kumar, V., Ricco, M.L., Bergman, R.D., Nepal, P., and Poudyal, N.C. (2024). Environmental impact assessment of mass timber, structural steel, and reinforced concrete buildings based on the 2021 international building code provisions. Build. Environ. 251: 111195.
- Lai, Y., Liu, X., Davies, M., Fisk, C., Holliday, M., King, D., Zhang, Y., and Willmott, J. (2024). Characterisation of wood combustion and emission under varying moisture contents using multiple imaging techniques. Fuel 373: 132397.
- Li, J.P., Han, X., Yao, S.S., Guo, D.K., and Chu, F.X. (2025). Reinforcing flame retardancy, dimensional stability, and high strength of wood for structural applications through surface densification and chemical modification. Ind. Crop. Prod. 223: 120175.
- Li, Y., Yao, T., Zhu, Y., Liu, S.Q., Shu, Z.J., Hasanagić, R., Leila, F., and Chu, D.M. (2024). Thermal modification intensity of heat-treated poplar wood. Part 2: characterization and predication from outside to core layers. Drv. Ind. 75, https://doi.org/10.5552/drvind.2024.0126.
- Luo, C.M., Hou, S.Y., Mu, J., and Qi, C.S. (2024). How does phosphoric acid affect the hygroscopicity and chemical components of poplar thermally modified at low temperatures? Wood Sci. Technol. 58: 699-723.
- Östman, B., Brandon, D., and Frantzich, H. (2017). Fire safety engineering in timber buildings. Fire Safety J. 91: 11-20.

- Özkan, O.E., Temiz, A., Tor, Ö., and Vurdu, H. (2022). Effect of post-heat treatment on fire retardant treated wood properties. Holzforschung 76: 645-657.
- Sauerbier, P., Mayer, A.K., Emmerich, L., and Militz, H. (2020). Fire retardant treatment of wood-state of the art and future perspectives. In: Wood & fire safety: proceedings of the 9th international conference on wood & fire safety 2020, 9. Springer International Publishing, pp. 97–102.
- Soula, M., Samyn, F., Duguesne, S., and Landry, V. (2024). Impact of surface delignification on fire retardancy of wood treated with polyelectrolyte complexes. Holzforschung 78: 244-256.
- Tan, K., Wang, Y., Li, X., Mou, Q., Deng, L., Peng, J., and Li, X. (2024). Surface layer reinforcement modification for wood with high strength and flame retardancy performances. Constr. Build. Mater. 450: 138672.
- Tang, J., Zhan, T.Y., Li, Z., Jiang, J.L., and Lyu, J.X. (2025). Optimization of dimensional stability and mechanical performance of thermally modified wood using cyclic-gradient thermal treatment. Constr. Build. Mater. 458: 139596.
- Tang, T., Chen, X.F., Zhang, B., Liu, X.M., and Fei, B.H. (2019). Research on the physico-mechanical properties of Moso bamboo with thermal treatment in tung oil and its influencing factors. Materials 12: 599.
- Wang, Y.J., Peng, Y., and Cao, J.Z. (2021). Analysis of microstructure and chemical components of southern pine during initial brown-rot decay. J. Beijing For. Univ. 43: 138-144.
- Wang, Y.W., Huang, R.F., and Zhang, Y.M. (2012). Surface densification and heat fixation of Chinese white poplar by hydrothermal control. Chin. Wood Ind. 26: 18-21.

- Wang, Y.Y., Li, Y.Q., Zhu, W.B., and Fu, S.Y. (2024). Strong and fire-resistant bamboo enabled by densification and boron nitride/graphene oxide nanocoating. Ind. Crop. Prod. 212: 118292.
- Wu, M.T., Hötte, C., Karthäuser, J., and Militz, H. (2025). Fire behavior of thermally modified pine (Pinus sylvestris) treated with DMDHEU and flame retardants: from small scale to SBI tests. Holzforschung
- Xu, Z.H., Zhao, W.J., Yan, L., Tang, X.Y., Feng, Y.W., and Wang, Z.Y. (2023). Processing of *Pinus sylvestris* L. into a heat-insulating, thermally stable, and flame-retarded material by combining the flame-retardant impregnation and densification treatment. Holzforschung 77: 762-775.
- Yang, H.P., Yan, R., Chen, H.P., Lee, D.H., and Zheng, C.G. (2007). Characteristics of hemicellulose, cellulose and lignin pyrolysis. Fuel 86: 1781_1788
- Yue, K., Wu, J., Xu, L., Tang, Z., Chen, Z., Liu, W., and Wang, L. (2020). Use impregnation and densification to improve mechanical properties and combustion performance of Chinese fir. Constr. Build. Mater. 241: 118101.
- Zhang, X., Fan, Q., Chen, C., Hao, X., Liu, Z., Ou, R., and Wang, Q. (2023). Enhanced mechanical performance and fire resistance of poplar wood: unilateral surface densification assisted with N/P doped acrylic resin impregnation. Constr. Build. Mater. 398: 132470.
- Zhou, Y., Qiu, W.X., Zhou, P.H., Wang, Z.Y., Zhang, X.N., Mao, X.Y., and Bu, R.W. (2024). Influences of species and density on the horizontal flame spread behavior of densified wood. Buildings 14: 620.